

# Molecular dynamics simulation of cell membrane pore sealing

Lili Zhang<sup>a,b</sup>, Zesheng Zhang<sup>c</sup>, Mehrdad Negahban<sup>c</sup>, Antoine Jérusalem<sup>a,d</sup>

<sup>a</sup>*University of Oxford, Department of Engineering Science, Oxford, OX1 3PJ, UK*

<sup>b</sup>*Current affiliation: University of Cambridge, Department of Engineering, Cambridge, CB2 1PZ, UK*

<sup>c</sup>*University of Nebraska-Lincoln, Department of Mechanical and Materials Engineering, Lincoln, NE 68588, USA*

<sup>d</sup>*Corresponding Author: antoine.jerusalem@eng.ox.ac.uk*

---

## Abstract

Biological membranes play a pivotal role in almost all cellular phenomena as highly versatile physiological and functional platforms for signalling and interacting lipids and proteins. Membrane integrity can be disrupted by diseases, mechanical trauma, and therapeutic processes, potentially causing deleterious effects including cell death. Membrane perforation, purposely-induced or undesired, is a basic perturbation to membrane's structural integrity, and can significantly influence a cell membrane's biomechanical and biophysical properties. However, the molecular mechanisms by which membrane pores dynamically respond to various loading conditions are still not well understood. By combining biomolecular simulations with multiscaling tools, this study quantitatively examines the dynamics of membrane pore sealing process at atomistic resolution in consistence with continuum mechanics concepts. Here, we consider hydrated lipid bilayer membranes with circular pores of various diameters ( $\sim 5 - 120$  Å) under constant pressure (1 atm) and temperature (310 K). Over the course of rapidly evolving sealing events, the continuum-like deformation characteristics of membranes are characterised based on molecular dynamics simulation results. We find that the membrane's areal strain histories exhibit appreciable sensitivity to the pore sizes, and that the membrane's out-of-plane strain evolution reflects its key structural alterations observed in the simulations. Water permeation is explored by quantifying the number of water molecules transferred from their initial layers through the pore to the opposite sides. Under the applied sealing conditions, our results suggest that both the water transport and time duration of membrane sealing markedly depend on the pore sizes. This work provides a computational framework aimed at probing transient biomolecular/cellular processes and

providing insights into the mechanistic underpinnings of post-poration molecular transport to further manipulate/control them for biomedical applications.

*Keywords:* cell membrane, poration, molecular dynamics, multiscale modelling

---

## 1. Introduction

Cell membranes play a pivotal role in nearly all cellular processes by, e.g., protecting the cell from the extracellular environment and participating directly in cell signalling, transport, and ion conductivity [1, 2]. Membrane compositional and structural alterations have been directly associated with a variety of diseases (e.g., cancer and neurodegenerative disorders) [3, 4, 5, 6, 7, 8, 9, 10, 11], injuries (e.g., traumatic brain injury and spinal cord injury) [12, 13, 14, 15, 16, 17], and therapeutics [18, 19, 20, 2]. These alterations can significantly disturb the membrane integrity, in turn causing changes in the cell's biochemomechanical properties [21, 22, 23]. As a result, cell membrane complexes have emerged as novel pharmacological and mechanical targets for a number of disease treatments [19, 20, 2].

Membrane perforation is one of the most fundamental damaging modes for cells and can be formed by several means: e.g., by directly exerting mechanical forces (such as shear stress [13] and biaxial stretching [24]) on cells, or by exposing cells to external acoustic/electric fields. In particular, membrane pores are purposely induced for therapeutic applications by imposing acoustic fields (a process termed sonoporation) such as ultrasound [25, 26, 27] and shock waves [28, 29, 30, 31, 32, 33, 23], or by applying electric fields (a process termed electroporation) [34, 35, 36, 37] to cells. These processes are used to temporarily enhance membrane permeability to allow therapeutic macromolecules in the surrounding medium to diffuse into cells, providing a means for acoustic/electric-field-mediated therapeutic drug delivery or gene transfer. In the case of neurons, mechanically-induced membrane poration has been reported to cause deleterious effects, such as axonal beading, localised cytoskeletal damage [13], unregulated ionic flux, and neuronal apoptosis as observed in traumatic brain injury and spinal cord injury [12, 15]. One of the mechanical hypotheses in neurodegenerative diseases research is that damaged neuronal membranes due to the loss of membrane elasticity can lead to an escape of cytoplasm from the neurons into the extracellular space [38]. This outflow has even been suggested as an important factor in the development of plaques and

tangles in the context of dementia [38].

Given their pathophysiological and therapeutic relevance, membrane pore formation and sealing have been extensively studied both in experimental settings [34, 36, 37, 12, 15, 26, 27, 24] and computer simulations [39, 40, 41, 42, 43, 44, 45, 46, 47, 48, 49, 23, 50, 16, 51, 52, 17, 53], where the *in silico* efforts have primarily focussed on detecting and identifying pore generation under different loading conditions. Yet, an atomic-resolution quantitative picture delineating the rapid, transient pore closure process in a manner consistent with continuum mechanics concepts is still lacking. To this end, we integrate atomistic simulations with our previously developed multiscaling framework [54, 55], which is in consistence with the fundamental continuum mechanics framework, to probe the molecular mechanisms underlying pore sealing processes in a quantitative manner. More specifically, here we consider fully hydrated lipid bilayer membranes with empty circular pores of various diameters ( $\sim 5 - 120$  Å) at a constant pressure of 1 atm and a constant temperature of 310 K. The discrete atomic details of sealing dynamics are captured by all-atom molecular dynamics (MD) simulations, and the corresponding continuum-like deformation characteristics (in-plane areal strain and out-of-plane strain) of lipids adjacent to the pores are extracted through the “MinD” method [54]. We also attempt to investigate the dynamic interplay between water permeation and membrane sealing. This is achieved by quantifying water molecule transport from their initial layers through pores to the opposite sides. This approach provides a numerical framework able to exploit post-poration molecule diffusion, a phenomenon of particular importance in the context of drug delivery.

## 2. Material and methods

MD simulations have become a very powerful tool that has been employed to study the behavior of all kinds of microstructures. It essentially solves Newton’s second law of motion for trajectories of a system of interacting particles [56, 57]. With the recent dramatic advances in computational capability and performance, the use of MD simulation in biology has grown substantially [58, 59, 60]. One key challenge is to utilise molecular level simulations to quantitatively characterise biomechanical/biophysical properties of cellular components and elucidate their biological processes at atomistic resolution. In addition to high computatio-

nal demand, such efforts require consistent scaling methods aimed at connecting the discrete atomistic details obtained from MD simulations to simple, representative continuum-like quantities such as stress and strain.

In the following, we first describe the molecular models of cell membranes with various pore sizes, then introduce the MD simulation setup and validation. A brief summary of the method to extract continuum-like deformation gradient from MD simulation results is finally presented.

### *2.1. Molecular models and MD simulation setup*

We employ all-atom MD simulations and assign the additive all-atom CHARMM36 lipid force field [61] to the phospholipid bilayer membrane systems. The water molecules are explicitly described using the TIP3P water model. The short-range pairwise interactions include Lennard Jones and Coulombic interactions with an additional energy switching function that ramps the energy smoothly to zero between the inner cutoff distance (8 Å) and the outer cutoff distance (12 Å). The long-range Coulombic interactions (meaning each charge in the system interacts with charges in an infinite array of periodic images of the simulation domain) are computed by invoking a particle-particle particle-mesh solver [62]. Molecular structures of hydrated cell membrane complexes are constructed and visualised using VMD [63].

Figure 1a shows the molecular model for a patch of fully hydrated 1-palmitoyl-2-oleoyl-sn-glycero-3-phosphocholine (POPC) bilayer membrane (including 2,620 lipid molecules) with overall dimensions of about  $28.5 \times 28.4 \times 41.1 \text{ nm}^3$  containing 1,007,942 water molecules in total. A sequence of energy minimisation and equilibration runs (following the well-established membrane-protein MD simulation protocols [64] with appropriate modifications) is performed utilising NAMD [64]. In order for the MD model to reach biophysically representative molecular structures, the equilibrium simulation is completed by a run (*NPT* computation) at constant temperature (310 K) and constant pressure (1 atm) with periodic boundary conditions applied in three directions until stable simulation box dimensions are achieved.

The equilibrium surface area per lipid, one of the critical mechanical properties of biolo-

gical membranes, is calculated for the POPC bilayer patch as  $\sim 61.51 \text{ \AA}^2$  in agreement with the experimental values of  $64.3 \text{ \AA}^2$  and  $68.3 \text{ \AA}^2$  reported by Kučerka et al. [65, 66]. The mass density of the hydrated POPC bilayer membrane ( $\sim 1.01 \text{ g/cm}^3$ ) is slightly less dense than the experimentally measured density distribution ( $\sim 1.10 - 1.12 \text{ g/cm}^3$ ) [67] for single living erythrocytes. The structural features of the lipid head and tail groups are observed to remain statistically stable during the final phase of equilibration.

Building on the well-equilibrated lipid bilayer membrane, a circular pore is generated by removing the lipid molecules that are within a selected radius from the membrane’s central out-of-plane axis. The resulting pore’s wall is directly made up of lipid tails and thus is hydrophobic. It must be emphasised that the pore created here only serve as a simple idealised representation for the highly intricate, actual membrane pores induced by external mechanical loading (e.g., cavitation) or pathologies. Figure 1b schematically illustrates a patch of hydrated membrane with a central empty pore, which is the starting configuration of subsequent pore sealing MD simulations. Figure 1c depicts the molecular structure of POPC bilayer membrane with an empty pore of  $\sim 120 \text{ \AA}$  in diameter containing 2,175 lipid molecules in total. **Note that the overall sizes of the simulation boxes for large pores ( $\geq 100 \text{ \AA}$  in diameter) are the same: about  $28.5 \times 28.4 \times 41.1 \text{ nm}^3$ .**

For the purpose of reducing computational cost, moderate-sized membrane complexes (including 1,162 lipid molecules and 47,627 water molecules in total) are prepared following the same protocol and used for creating moderate-sized pores (with diameters  $\leq 90 \text{ \AA}$ ). **Note that the overall dimensions of the simulation boxes for the moderate-sized pores are the same: about  $19.77 \times 20.05 \times 7.23 \text{ nm}^3$ . The number of lipid and water molecules is chosen so that the overall system size is adequately large to (1) preclude any interaction between the membrane pore (in the central part of the simulation box) and its images due to the use of periodic boundary conditions; (2) cause no statistical changes to the pore’s behaviour when the simulation box boundaries are perturbed by adding/removing a small amount of water or lipid molecules at the boundaries. Another noteworthy option to reduce the system size (and thus to mitigate the computational cost) is to adopt different in-plane dimensions, for example, by varying the size of the bilayer patch proportionally to its pore’s area.**

The membrane pore sealing simulations are carried out utilising LAMMPS [68] whose

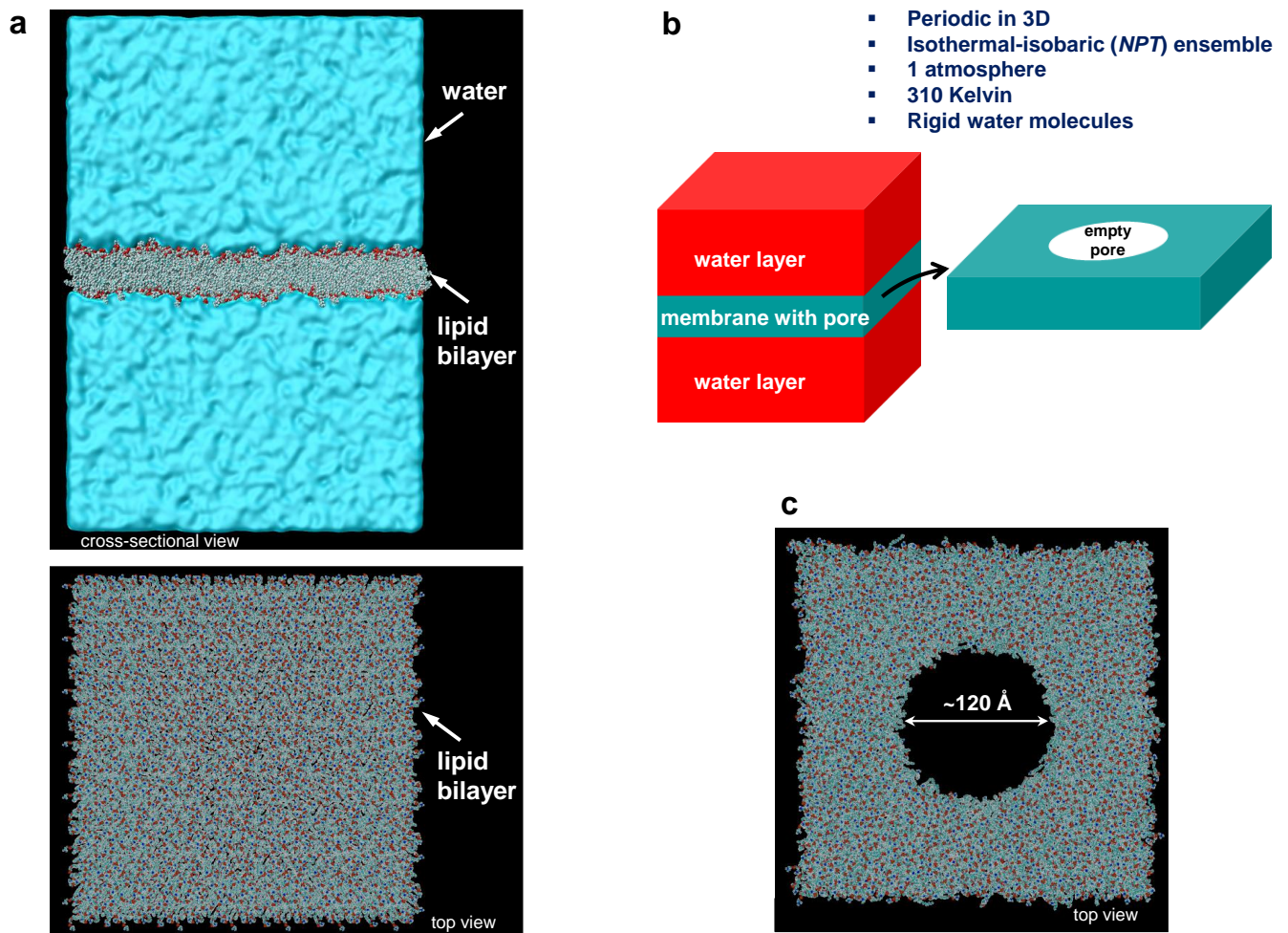


Figure 1: All-atom molecular models of hydrated cell membrane complexes: (a) patch of hydrated 1-palmitoyl-2-oleoyl-sn-glycero-3-phosphocholine (POPC) bilayer membrane (water molecules are drawn as QuickSurf, and lipids are represented as Lines); (b) schematic illustration of the MD implementation of membrane sealing with the simulated process starting with an empty circular pore; (c) patch of POPC bilayer membrane with a pore of  $\sim 120$  Å in diameter (water molecules are visually hidden for clarity).

initial configurations consist of two water layers and a patch of lipid bilayer with an empty pore (as shown in Figure 1b). The pore sealing process is implemented in a *NPT* computation at constant temperature (310 K) and pressure (1 atm) with periodic boundary conditions imposed in three dimensions. Time integration is performed with the Nose-Hoover style non-Hamiltonian equations of motion. Bond and angle constraints are applied to all water molecules (i.e., rigid water molecules) by the SHAKE algorithm to enable using a longer time step (here, 1 fs). The pairwise neighbor lists are updated every time step.

## 2.2. Multiscale method to extract continuum-like quantities from MD simulations

Classical “continuum mechanics” approaches offer a fundamental framework to quantitatively characterise and rationalise biomechanical processes and mechanisms associated with biological systems. A number of multiscaling methods have been developed or adapted to formulate “continuum mechanics” measures based on atomistic/molecular-level knowledge with the aim of linking the discrete atomistic/molecular scale to the continuum scale. Despite numerous research efforts, many open questions and challenges remain [69], particularly for biological systems where complex irregular structures are expected.

To this end, we have previously proposed a multiscale framework through which a continuum-like deformation gradient (the “MinD” method [54]), Cauchy stress (the “MinT-EE” method [54]), and “interaction stress” [55] can be constructed from MD simulation results in a manner consistent with continuum mechanics concepts. The “MinD” and “MinT-EE” methods are based on the idea of minimising the difference between MD measures for deformation and traction, and their continuum counterparts. The fundamental idea of defining “interaction stress” lies in constructing a continuum stress field that is equivalent (i.e., producing the same resultant force, moment and power) to the discrete particle forces determined from the MD simulations. It is important to note that these procedures are independent of the type of interactions and thus applicable to both all-atom and coarse-grained MD simulations. Also, these methods are motivated by the need to quantitatively characterise continuum-like mechanical signatures of any arbitrary parts of an inhomogeneous system subject to thermodynamically non-equilibrium processes. It is thus particularly appropriate for probing the dynamics of biological systems under transient loading conditions such as membrane sealing.

Here we focus specifically on examining the first-order deformation characteristics and thus only summarise the derivation pertaining to this aspect (see the “MinD” method [54] for building higher-order deformation gradients). The software package that implements the “MinD” method to extract continuum-like deformation gradients from MD simulation outputs is available at *UNL Digital Commons* (<http://digitalcommons.unl.edu/mechengfacpub/207/>) and is released under a general use license. Natively, the software directly supports LAMMPS dump file format. In the following, we briefly summarise the method, see Ref. [54] for more

details.

Let  $\Omega$  denote an arbitrarily selected group of particles, for example, a subdomain of a protein molecule. The total mass  $m$  and position of the centre of mass  $\mathbf{R}_{CM}$  of the group in the reference configuration are given, respectively, by

$$m = \sum_{i \in \Omega} m_i, \quad (1)$$

$$\mathbf{R}_{CM} = \frac{1}{m} \sum_{i \in \Omega} m_i \mathbf{R}_i, \quad (2)$$

where  $m_i$  and  $\mathbf{R}_i$  denote the mass and the position vector of particle  $i \in \Omega$  in the reference configuration, respectively. The relative position of particle  $i$  with respect to the centre of mass  $CM$  is denoted by  $\Delta \mathbf{R}_i$  and given by

$$\Delta \mathbf{R}_i = \mathbf{R}_i - \mathbf{R}_{CM}. \quad (3)$$

To make the transition from molecular motion to continuum deformation, we assume that a motion function, similar to that in continuum mechanics, exists that maps points from their reference (undeformed) configuration to their current (deformed) configuration. This motion function is written in the traditional manner as  $\mathbf{x}(\mathbf{X}, t)$ , where  $\mathbf{x}$  is the current location at time  $t$  of the continuum particle that is at location  $\mathbf{X}$  in the reference configuration. This mapping allows us to construct a Taylor series expansion at any point  $\mathbf{X}_o$  as

$$\begin{aligned} \mathbf{x}(\mathbf{X}, t) = & \mathbf{x}(\mathbf{X}_o, t) + \mathbf{F}(t) \cdot (\mathbf{X} - \mathbf{X}_o) + \frac{1}{2} \mathbf{F}^{(2)}(t) : [(\mathbf{X} - \mathbf{X}_o) \otimes (\mathbf{X} - \mathbf{X}_o)] \\ & + \frac{1}{3!} \mathbf{F}^{(3)}(t) : [(\mathbf{X} - \mathbf{X}_o) \otimes (\mathbf{X} - \mathbf{X}_o) \otimes (\mathbf{X} - \mathbf{X}_o)] + \dots, \end{aligned} \quad (4)$$

where  $\mathbf{F}(t)$  and  $\mathbf{F}^{(n)}(t)$  respectively denote the first-order and the  $n^{th}$ -order spatial gradients with respect to  $\mathbf{X}$  of the motion function evaluated at  $\mathbf{X}_o$ . The tensor operators “ $\cdot$ ”, “ $:$ ”, “ $:$ ” and “ $\otimes$ ” respectively denote the dot product, double and triple dot products, and the dyadic product.

In this study we focus on a linear mapping (i.e., the expansion includes up to the first-order gradient, with the higher-order terms truncated) expanded around the centre of mass



$\mathbf{R}_{CM}$ . As expected, by introducing the reference location of any particle into this continuum motion function, one obtains a current location  $\mathbf{x}(\mathbf{R}_i, t) = \mathbf{x}(\mathbf{R}_{CM}, t) + \mathbf{F}(t)\Delta\mathbf{R}_i$  that is not exactly where the actual particle is ( $\mathbf{r}_i$ ). Let us denote this difference (error) for particle  $i$  as  $\Delta_i$  so that

$$\mathbf{r}_i = \mathbf{x}(\mathbf{R}_i) + \Delta_i. \quad (5)$$

The aim of the method is to match as close as possible the motions seen in the MD simulation with that from the continuum motion function. To this end, we use a least-square minimisation process to minimise the difference between the MD and continuum measures. The total error for the group can be evaluated by introducing an overall error function  $R$  that sums the errors of all the individual particles:

$$R = \frac{1}{2} \sum_{i \in \Omega} m_i (\Delta_i \cdot \Delta_i), \quad (6)$$

where the particle mass  $m_i$  is used as the weighting factor associated with particle  $i$ . Our task is to select a vector  $\mathbf{x}(\mathbf{R}_{CM})$  and a tensor  $\mathbf{F}$  that minimise the global error  $R$ . As is common in data regression, the optimal fit is the one for which the variation in  $R$  is zero for all possible variations of  $\mathbf{x}(\mathbf{R}_{CM})$  and  $\mathbf{F}$ . This corresponds to finding the stationary point of the overall error function, eventually leading to [54]:

$$\mathbf{F} = \left( \sum_{i \in \Omega} m_i (\mathbf{r}_i - \mathbf{x}_{CM}) \otimes \Delta\mathbf{R}_i \right) \left( \sum_{i \in \Omega} m_i \Delta\mathbf{R}_i \otimes \Delta\mathbf{R}_i \right)^{-1}, \quad (7)$$

where  $\mathbf{x}_{CM}$  is the current centre of mass of the selected system. This continuum-like deformation gradient allows us to define right and left Cauchy stretch tensors  $\mathbf{C} = \mathbf{F}^T \cdot \mathbf{F}$  and  $\mathbf{B} = \mathbf{F} \cdot \mathbf{F}^T$ , and the associated Green-Lagrange strain  $\mathbf{E}$  given by

$$\mathbf{E} = \frac{1}{2}(\mathbf{C} - \mathbf{I}). \quad (8)$$

This continuum measure is used in the following to evaluate the out-of-plane strain, as well

as the areal strain given by

$$\varepsilon_A \equiv \frac{dA}{dA_o} - 1 = \sqrt{\det(\mathbf{C}) \hat{\mathbf{N}} \cdot (\mathbf{C}^{-1} \cdot \hat{\mathbf{N}})} - 1, \quad (9)$$

where  $dA_o$  denotes an infinitesimal area with unit normal vector  $\hat{\mathbf{N}}$  in the reference configuration, and  $dA$  denotes the corresponding area in the current configuration.

### 3. Results

In order to set the stage for analysing the membrane's deformation characteristics during the sealing process, representative membrane groups are selected and tracked throughout the simulation. In the following, the group LP denotes lipid molecules adjacent to the pore, and their hydrophilic head domains are gathered as the group LPHeads. Figure 2 shows an ongoing sealing process for a  $\sim 120$  Å-diameter pore up to 8.70 ns, where the motion of group LPHeads is traced. Figure 3 depicts the structural evolution of group LP and group LPHeads during a  $\sim 90$  Å-diameter pore sealing from an initial empty pore up to a fully sealed configuration. Figures 2 and 3 also display the movement of water molecules over the course of pore sealing, including permeation through the pore, formation of a water bridge, transfer from one side of membrane to the other, and push-back out of the pore when it completely seals in the latter case.

Complete membrane sealing is achieved and captured under the simulated condition for pores with diameters less than or equal to  $\sim 90$  Å. For large pores (diameter  $\geq 100$  Å), the ongoing sealing dynamics is obtained for the initial 8.70 ns. The time evolution of membrane's in-plane areal strain (using Equation (9)) and out-of-plane strain (using Equation (8)) during the sealing process is presented in Figure 4 for various pore sizes. For moderate-sized pores (diameter  $\leq 90$  Å), Figures 4a and b respectively reveal the areal strain and out-of-plane strain histories for group LP (i.e., surrounding lipids) covering the whole sealing event. There are two primary stages in the evolution of areal strains: a gradual drop from the initial zero strain (suggesting in-plane compressive deformations) followed by a stable plateau indicating that the lipids under consideration have reached a local equilibrium conformation. This trend can be approximated with a Prony series ( $f(t) = ae^{-\tau_s^{-1}t} + xe^{-\tau_f^{-1}t} - z$ ) whose

corresponding fitted curves are also given in Figure 4a. The slow relaxation time  $\tau_s$  and the long-term areal strain  $z$  both vary with the pore size. It takes a longer time (where  $\tau_s$  increases exponentially with pore size) and greater areal contraction (where  $z$  increases logarithmically with pore size) for a larger pore to seal, as could be expected.

Figure 4b shows how the out-of-plane strains of group LP evolve over time for the moderate-sized pores. This response can be described in three primary stages: an immediate drop from initial zero strain to a negative strain (i.e., thickness is reduced), then an increase to a positive strain (i.e., membrane becomes thicker than original) followed by a plateau (i.e., a local equilibrium conformation is reached). The alteration of membrane thickness is closely related to the motion of water molecules that hydrate their hydrophilic phosphate heads. Some of the lipid heads at the edge of a pore travel with water toward the pore's inner space to form a hydrophilic pore wall (see Figures 2 and 3), which might cause the thickness drop. With the progress of sealing, water molecules together with lipid heads are gradually pushed out of the pore until the membrane is fully sealed (see Figure 3). The rearrangement of lipids possibly leads to the final thickness increase.

Figure 4c reveals the deformation of lipid heads (group LPHeads) in the large pore systems for the first 8.70 ns. The areal and out-of-plane strains follow similar trends to those seen in the moderate-sized systems, and no plateaus are achieved within the considered time frame indicating that the sealing is still in progress.

The interplay between water and pore is probed here by tracing the motion of water molecules during membrane sealing. For pores with diameters less than or equal to  $\sim 20$  Å, nearly no water molecules enter the pore, thus no water permeates through the pore to the opposite side. Possible mechanisms could be that the attractive forces for closing the pore as well as the repulsive forces exerted on water from the pore wall (consisting of hydrophobic lipid tails) favour a direct pore closure instead of water permeation. For pores with diameters greater than or equal to  $\sim 30$  Å, a clear formation of water bridge through the pore is observed (see Figures 2 and 3) and the water transport across the bilayer can then be estimated. In the fully sealed configuration (for pore with diameter  $\leq 90$  Å), the number of water molecules that have travelled from their original layer to the opposite layer is evaluated, see Figure 5. This number exhibits an approximately linear dependence on the

pore’s diameter in the range of  $\sim 40 - 90$  Å. Figure 5 also includes the approximate number of water molecules that are in the process of penetrating through large pores (diameter  $\geq 100$  Å) to the opposite sides (including the water that has entered the opposite parts of the pore) at time  $t = 8.70$  ns. It should be noted that these numbers only provide a quantitative snapshot of a highly dynamic, fast evolving process and thus are not sufficient to predict any long-term water transport information.

Figure 6a reveals the progression of the configurations of water molecules within the pore domains for various initial sizes during membrane sealing. Representative close-ups of water in the pore highlight the interplay between water transport and pore sealing: penetrating the empty pore in a non-uniform, non-regular shaped manner, forming transmembrane, cylindrical-like, “continuous” water bridge, and eventually being expelled from the pore interior in a rather random-shaped manner. This process is quantitatively depicted in Figure 6b, where the time evolution of the total amount of water molecules within the pore domain also indicates its marked pore-size dependence.

Computer simulations have already been leveraged to provide molecular level details of pore formation and closure in cell membranes. Despite distinct differences in the details of membrane’s pore opening, composition, and structure, the underlying structural feature of the pores is conserved [43, 53]: toroidal-shaped with lipid headgroups lining the pore’s wall as observed in this study. In contrast, the dynamics of pore closure has been shown to largely depend on the pore forming process, and the composition and structure of the lipid bilayer. Bennett et al. [70] used atomistic MD simulations to estimate pore closure times for three model membranes: DPPC bilayer (closure time 6.6 ns), DMPC bilayer (closure time 123 ns), and DLPC bilayer (closure time  $> 500$  ns), where the pore was formed by moving the phosphate of a single lipid to the centre of the bilayer. Tarek [71] performed MD simulations of DMPC bilayers porated by applying external transmembrane electric fields, and reported the complete resealing of the bilayers within  $2 - 4$  ns. Koshiyama et al. [46] reported that the maximum lifetime of a pore (with about 1.4 nm in diameter) was about 32 ns in their united-atom MD study, where the pore was spontaneously induced by 800 water molecules pre-inserted in the hydrophobic region of an intact DPPC bilayer. Via real-time 3D confocal microscopy (millisecond resolution) measurements, Helfield et

al. [27] provided evidence that ultrasound-triggered microbubbles directly resulted in the immediate generation of membrane pores (with pore area of  $\sim 660 \mu\text{m}^2$ ) that completely resealed within about 12 minutes. Yuan et al. [26] developed an experimental microfluidic system to demonstrate that pinpoint membrane poration could be produced by laser-induced tandem bubbles (TBs) at the single cell level, which is prevalent in therapeutic ultrasound applications. Poration was monitored by membrane impermeant propidium iodide uptake from the culture medium. The recovery of cell membrane pore was recorded using a high-speed video camera operated at 20  $\mu\text{s}$  interframe time at the optical resolution of about 0.4  $\mu\text{m}$ . The authors reported that the repairable poration resealed within 10 s following the TB treatment.

These previous studies highlight the following conundrum: i) a direct simulation of small-sized pores sealing is at best very complex and beyond the reach of our computational capabilities for large-sized pores, and ii) cell membrane’s nanometer-sized perforation/sealing processes on the nanosecond time scale still cannot be directly resolved/observed by using current experimental techniques (with submicrosecond time resolution and submicrometer spatial resolution). However, by extrapolating the continuum-like sealing characteristics described for the moderate-sized pores (see Figure 4a) to large-sized pores (and thus assuming that they fully seal with time), the slow relaxation time  $\tau_s$  and the long-term areal strain  $z$  for group LP (the lipids encompassing the large pores) can then be respectively predicted to reach:  $\tau_s \approx 9.1 \text{ ns}$  and  $z \approx 0.78$  for pore of  $\sim 100 \text{ \AA}$  in diameter, and  $\tau_s \approx 13.5 \text{ ns}$  and  $z \approx 0.81$  for pore of  $\sim 120 \text{ \AA}$  in diameter. This however, assumes complete resealing, which can only be assessed on much larger time scales. Direct experimental evidence capable of elucidating membrane’s nanometer-sized pore formation and closure is thus greatly needed.

#### 4. Discussion

The past decades have seen significant progress in atomic-level biomolecular simulations as a result of the continuing improvements in computer hardware, software, and simulation methodologies [59]. Major breakthroughs in structural biology and computational biology have provided extraordinary opportunities for using MD simulations to probe fundamental

biomolecular processes pertaining to physiology, pathology, injury, and therapy at spatio-temporal scales that are difficult to access experimentally. These rapidly expanding MD applications motivate the need for innovative scaling methods aimed at linking biomechanical information across different length scales so as to provide insights into the molecular mechanisms underlying sophisticated biological phenomena involved in diseases, injuries, and treatments.

To this end, this study has applied our previously proposed multiscaling framework [54, 55] to quantitatively characterise the highly dynamic membrane sealing event in a manner consistent with classical continuum mechanics concepts. Here we have focussed on POPC bilayer membranes with empty circular pores (see Figure 1) of various sizes ( $\sim 5 - 120$  Å in diameter), which serve as an idealised representation for membrane poration induced by mechanical trauma, diseases or therapeutics. The membrane’s structural alterations and water permeation over the course of pore sealing are captured in full atomic detail (see Figures 2 and 3), and the corresponding deformation characteristics are quantified via the “MinD” method [54]. The membrane’s fully sealed conformations are achieved for the moderate-sized pores (diameters  $\leq 90$  Å) whose complete in-plane areal and out-of-plane strain histories (see Figures 4a-b) quantitatively mirror their characteristic structural rearrangements in concert with water transport observed in simulations. The areal strain evolution can be approximately described with Prony series whose slow relaxation time  $\tau_s$  and long-term constant  $z$ , as an approximate measure of the sealing characteristics, exhibit their dependence on pore’s size. The hydrophilic phosphate heads at a pore’s edge move collectively with water molecules inward and outward, which might be the cause of the alteration of membrane thickness in the sealing process. In the sealed configurations, the out-of-plane strains remain positive, suggesting that the membranes are thicker than in their initial states. After membrane sealing is completed, further examination could study whether such change in thickness debilitates the membrane’s functions, e.g., protein-lipid interactions and membrane signalling cascades.

Water permeation is quantified by estimating how many water molecules have diffused across the membrane (see Figure 5). An approximately linear relation is obtained showing the dependence of the number of transported water molecules on the pore diameters in

the range of  $\sim 40 - 90$  Å. Note that no water transport is observed for pores with diameters  $\leq 20$  Å under the current sealing conditions. Additional work could focus on whether additional loading conditions during resealing could modulate water transport through specific-sized pores, for example, by potentiating water diffusion through very small pores, or averting/minimising water penetration in the presence of moderate/large pores.

For large pores (diameter  $\geq 100$  Å), the ongoing sealing dynamics is captured for the initial 8.70 ns. The deformation features of lipid heads (see Figure 4c) and motion of water molecules (see Figures 2, 5 and 6) evolve in a similar way as observed in their moderate-sized counterparts. Due to the intricate interplay between membrane sealing and water transport, it is difficult to postulate whether these large pores could achieve their completely sealed conformations or eventually reach their local equilibrium configurations where pores filled with water maintain open and stable, but one would assume a similar evolution as in the moderate-sized pores.

It is important to emphasise the limitations of our study, which should be addressed by further investigations within a similar computational framework. **First, all-atom MD simulations of biological systems are computationally demanding, thus placing restrictions on the achievable spatial and temporal scales. For the large pore system (with  $\sim 120$  Å in diameter),  $\sim 588,000$  CPU core hours are required to cover the initial 8.70 ns of the sealing process. A variety of techniques, such as coarse-graining (e.g., residue-based coarse-graining and shape-based coarse graining) and enhanced sampling (see reviews in Ref. [72, 73]), can be utilised to probe the biological events occurring on the tens of nanoseconds to microseconds time scale inaccessible to direct large-scale all-atom MD simulations.** Next, the complexity of biological systems is further compounded by structural and compositional alterations caused by injury/disease/therapeutic processes. This poses additional challenges in accurately simulating cellular response to in vivo chemomechanical environments. Here we have adopted several major simplifications in the simulation settings in order to set up a relatively general and simple case as well as to alleviate the inherent computational complexities. Based on equilibrated membrane complexes, circular pores were created by removing lipid molecules within specified domains. Thus any possible residual stresses, residual strains or complex geometries that may be induced by actual membrane perforation processes are not taken into

account. Also note that the sealing dynamics starts with an empty pore rather than a pore pre-filled with water. This is purposely designed to probe the transient, non-equilibrium process where pore sealing and water transport are implicated simultaneously. As one of the most basic loading modes, the simulated conditions (i.e., constant pressure at 1 atm and constant temperature at 310 K) is arguably not fully representative of in vivo environments where intertwined mechanical and electric fields are expected during the membrane poration/sealing processes. Future studies should explore how to use different external stimuli (such as inhomogeneous and/or time varying pressure and electric fields) to mediate the concurrent membrane sealing and water (and/or drug molecules) transportation process. The molecular mechanisms by which water molecules mechanically interact with membrane pores during sealing will be investigated next and will provide additional mechanistic insights into their complex interplay.

Albeit simplistic, this work provides a computational foundation for quantitatively examining the dynamics of membrane sealing in full atomic detail. It potentially offers avenues for the development of tailored mechanical/electric fields to manipulate membrane perforation/sealing events and to control water (and/or drug molecules) transport. This has direct implications for (i) promoting membrane repair/recovery from mechanical trauma seen in traumatic brain injury or spinal cord injury, (ii) potentiating electroporation/sonoporation effects for drug delivery across cell membranes, and (iii) providing a deeper understanding of membrane poration as induced by cavitation phenomena.

## Acknowledgements

L.Z. and A.J. acknowledge funding from the European Research Council under the European Union Seventh Framework Programme (FP7 2007-2013)/ERC Grant Agreement No. 306587. Z.Z. and M.N. acknowledge funding from the US Army Research Laboratory Cooperative Agreement No. W911NF-04-2-00-11 through Contract No. W911NF-11-D-0001-0094. The authors would like to acknowledge the use of the University of Oxford Advanced Research Computing (ARC) facility in carrying out this work (<http://dx.doi.org/10.5281/zenodo.22558>).



## Reference

## References

- [1] S. J. Singer and G. L. Nicolson. The fluid mosaic model of the structure of cell membranes. *Science*, 175(4023):720–731, 1972.
- [2] P. V. Escribá, X. Busquets, J. Inokuchi, G. Balogh, Z. Török, I. Horváth, J. L. Harwood, and L. Vígh. Membrane lipid therapy: modulation of the cell membrane composition and structure as a molecular base for drug discovery and new disease treatment. *Progress in Lipid Research*, 59:38–53, 2015.
- [3] T. R. Triton and G. Yee. The anticancer agent adriamycin can be actively cytotoxic without entering cells. *Science*, 217(4556):248–250, 1982.
- [4] P. V. Escribá, M. Sastre, and J. A. García-Sevilla. Disruption of cellular signaling pathways by daunomycin through destabilization of nonlamellar membrane structures. *Proceedings of the National Academy of Sciences of the United States of America*, 92(16):7595–7599, 1995.
- [5] M. Simons, P. Keller, B. De Strooper, K. Beyreuther, C. G. Dotti, and K. Simons. Cholesterol depletion inhibits the generation of beta-amyloid in hippocampal neurons. *Proceedings of the National Academy of Sciences of the United States of America*, 95(11):6460–6464, 1998.
- [6] B. Grziwa, M. O. W. Grimm, C. L. Masters, K. Beyreuther, T. Hartmann, and S. F. Lichtenthaler. The transmembrane domain of the amyloid precursor protein in microsomal membranes is on both sides shorter than predicted. *Journal of Biological Chemistry*, 278(9):6803–6808, 2003.
- [7] G. Avila-Martin, I. Galan-Arriero, J. Gomez-Soriano, and J. Taylor. Treatment of rat spinal cord injury with the neurotrophic factor Albumin-Oleic Acid: translational application for paralysis, spasticity and pain. *PLoS ONE*, 6(10):e26107, 2011.

- [8] G. Avila-Martin, I. Galan-Arriero, A. Ferrer-Donato, X. Busquets, J. Gomez-Soriano, P. V. Escribá, and J. Taylor. Oral 2-hydroxyoleic acid inhibits reflex hypersensitivity and open-field-induced anxiety after spared nerve injury. *European Journal of Pain*, 19(1):111–122, 2015.
- [9] V. Balanzá-Martínez, G. R. Fries, G. D. Colpo, P. P. Silveira, A. K. Portella, R. Tabarés-Seisdedos, and F. Kapczinski. Therapeutic use of omega-3 fatty acids in bipolar disorder. *Expert Review of Neurotherapeutics*, 11(7):1029–1047, 2011.
- [10] R. Alemany, O. Vögler, S. Terés, C. Egea, C. Baamonde, F. Barceló, C. Delgado, K. H. Jakobs, and P. V. Escribá. Antihypertensive action of 2-hydroxyoleic acid in SHRs via modulation of the protein kinase A pathway and Rho kinase. *Journal of Lipid Research*, 47(8):1762–1770, 2006.
- [11] S. Terés, G. Barceló-Coblijn, M. Benet, R. Álvarez, R. Bressani, J. E. Halver, and P. V. Escribá. Oleic acid content is responsible for the reduction in blood pressure induced by olive oil. *Proceedings of the National Academy of Sciences of the United States of America*, 105(37):13811–13816, 2008.
- [12] O. Farkas, J. Lifshitz, and J. T. Povlishock. Mechanoporation induced by diffuse traumatic brain injury: an irreversible or reversible response to injury? *Journal of Neuroscience*, 26(12):3130–3140, 2006.
- [13] D. Kilinc, G. Gallo, and K. A. Barbee. Mechanically-induced membrane poration causes axonal beading and localized cytoskeletal damage. *Experimental Neurology*, 212(2):422–430, 2008.
- [14] F. Li, C. U. Chan, and C. D. Ohl. Yield strength of human erythrocyte membranes to impulsive stretching. *Biophysical Journal*, 105(4):872–879, 2013.
- [15] B. K. Hendricks and R. Shi. Mechanisms of neuronal membrane sealing following mechanical trauma. *Neuroscience Bulletin*, 30(4):627–644, 2014.
- [16] Y. Sliozberg and T. Chantawansri. Damage in spherical cellular membrane generated

- by the shock waves: coarse-grained molecular dynamics simulation of lipid vesicle. *The Journal of Chemical Physics*, 141(18):184904, 2014.
- [17] E. Y. Lau, M. L. Berkowitz, and E. Schwegler. Shock wave-induced damage of a protein by void collapse. *Biophysical Journal*, 110(1):147–156, 2016.
- [18] W. A. Lam, M. J. Rosenbluth, and D. A. Fletcher. Chemotherapy exposure increases leukemia cell stiffness. *Blood*, 109(8):3505–3508, 2007.
- [19] G. Barceló-Coblijn, M. L. Martin, R. F. M. de Almeida, M. A. Noguera-Salvà, A. Marcilla-Etxenike, F. Guardiola-Serrano, A. Lüth, B. Kleuser, J. E. Halver, and P. V. Escribá. Sphingomyelin and sphingomyelin synthase (SMS) in the malignant transformation of glioma cells and in 2-hydroxyoleic acid therapy. *Proceedings of the National Academy of Sciences of the United States of America*, 108(49):19569–19574, 2011.
- [20] S. Terés, V. Lladó, M. Higuera, G. Barceló-Coblijn, M. L. Martin, M. A. Noguera-Salvà, A. Marcilla-Etxenike, J. M. García-Verdugo, M. Soriano-Navarro, C. Saus, U. Gómez-Pinedo, X. Busquets, and P. V. Escribá. 2-Hydroxyoleate, a nontoxic membrane binding anticancer drug, induces glioma cell differentiation and autophagy. *Proceedings of the National Academy of Sciences of the United States of America*, 109(22):8489–8494, 2012.
- [21] L. Weiss. Biomechanical interactions of cancer cells with the microvasculature during hematogenous metastasis. *Cancer and Metastasis Reviews*, 11(3):227–235, 1992.
- [22] S. Suresh. Biomechanics and biophysics of cancer cells. *Acta Biomaterialia*, 3(4):413–438, 2007.
- [23] M. O. Steinhauser and M. Schmidt. Destruction of cancer cells by laser-induced shock waves: recent developments in experimental treatments and multiscale computer simulations. *Soft Matter*, 10(27):4778–4788, 2014.
- [24] M. C. LaPlaca, M. C. Lessing, G. R. Prado, R. Zhou, C. C. Tate, D. Geddes-Klein, D. F. Meaney, and L. Zhang. Mechanoporation is a potential indicator of tissue strain

- and subsequent degeneration following experimental traumatic brain injury. *Clinical Biomechanics*, 0(0), 2018.
- [25] Z. Fan, H. Liu, M. Mayer, and C. X. Deng. Spatiotemporally controlled single cell sonoporation. *Proceedings of the National Academy of Sciences of the United States of America*, 109(41):16486–16491, 2012.
  - [26] F. Yuan, C. Yang, and P. Zhong. Cell membrane deformation and bioeffects produced by tandem bubble-induced jetting flow. *Proceedings of the National Academy of Sciences of the United States of America*, 112(51):E7039–E7047, 2015.
  - [27] B. Helfield, X. Chen, S. C. Watkins, and F. S. Villanueva. Biophysical insight into mechanisms of sonoporation. *Proceedings of the National Academy of Sciences of the United States of America*, 113(36):9983–9988, 2016.
  - [28] S. Bao, B. D. Thrall, R. A. Gies, and D. L. Miller. In vivo transfection of melanoma cells by lithotripter shock waves. *Cancer Research*, 58(2):219–221, 1998.
  - [29] R. F. Randazzo, C. G. Chaussy, G. J. Fuchs, S. M. Bhuta, H. Lovrekovich, and J. B. deKernion. The in vitro and in vivo effects of extracorporeal shock waves on malignant cells. *Urol Res.*, 16(6):419–426, 1988.
  - [30] J. C. Williams, J. F. Woodward, M. A. Stonehill, A. P. Evan, and J. A. McAteer. Cell damage by lithotripter shock waves at high pressure to preclude cavitation. *Ultrasound in Medicine & Biology*, 25(9):1445–1449, 1999.
  - [31] M. Delius and G. Adams. Shock wave permeabilization with ribosome inactivating proteins: a new approach to tumor therapy. *Cancer Research*, 59(20):5227–5232, 1999.
  - [32] T. Kodama, A. G. Doukas, and M. R. Hamblin. Shock wave-mediated molecular delivery into cells. *Biochimica et Biophysica Acta (BBA)-Molecular Cell Research*, 1542(1):186–194, 2002.
  - [33] R. Murata, K. Nakagawa, S. Ohtori, N. Ochiai, M. Arai, T. Saisu, T. Sasho, K. Takahashi, and H. Moriya. The effects of radial shock waves on gene transfer in rabbit chondrocytes in vitro. *Osteoarthritis and Cartilage*, 15(11):1275–1282, 2007.

- [34] E. Neumann and K. Rosenheck. Permeability changes induced by electric impulses in vesicular membranes. *The Journal of Membrane Biology*, 10(1):279–290, 1972.
- [35] J. C. Weaver and Y. A. Chizmadzhev. Theory of electroporation: a review. *Bioelectrochemistry and Bioenergetics*, 41(2):135–160, 1996.
- [36] M. P. Rols, C. Delteil, M. Golzio, P. Dumond, S. Cros, and J. Teissie. In vivo electrically mediated protein and gene transfer in murine melanoma. *Nature Biotechnology*, 16:168–171, 1998.
- [37] S. Mehier-Humbert and R. H. Guy. Physical methods for gene transfer: improving the kinetics of gene delivery into cells. *Advanced Drug Delivery Reviews*, 57(5):733–753, 2005.
- [38] H. Barz, U. Barz, and A. Schreiber. Neuronal impulse theory and Alzheimer’s disease. *Journal of Alzheimers Disease & Parkinsonism*, 4(1):1000134, 2014.
- [39] D. P. Tieleman, H. Leontiadou, A. E. Mark, and S. J. Marrink. Simulation of pore formation in lipid bilayers by mechanical stress and electric fields. *Journal of the American Chemical Society*, 125(21):6382–6383, 2003.
- [40] T. V. Tolpekina, W. K. den Otter, and W. J. Briels. Simulations of stable pores in membranes: system size dependence and line tension. *The Journal of Chemical Physics*, 121(16):8014–8020, 2004.
- [41] K. Koshiyama, T. Kodama, T. Yano, and S. Fujikawa. Structural change in lipid bilayers and water penetration induced by shock waves: molecular dynamics simulations. *Biophysical Journal*, 91(6):2198–2205, 2006.
- [42] R. A. Böckmann, B. L. de Groot, S. Kakorin, E. Neumann, and H. Grubmüller. Kinetics, statistics, and energetics of lipid membrane electroporation studied by molecular dynamics simulations. *Biophysical Journal*, 95(4):1837–1850, 2008.
- [43] S. J. Marrink, A. H. de Vries, and D. P. Tieleman. Lipids on the move: simulations of membrane pores, domains, stalks and curves. *Biochimica et Biophysica Acta (BBA)-Biomembranes*, 1788(1):149–168, 2009.

- [44] M. L. Fernández, G. Marshall, F. Sagués, and R. Reigada. Structural and kinetic molecular dynamics study of electroporation in cholesterol-containing bilayers. *The Journal of Physical Chemistry B*, 114(20):6855–6865, 2010.
- [45] J. Neder, B. West, P. Nielaba, and F. Schmid. Coarse-grained simulations of membranes under tension. *The Journal of Chemical Physics*, 132(11):115101, 2010.
- [46] K. Koshiyama, T. Yano, and T. Kodama. Self-organization of a stable pore structure in a phospholipid bilayer. *Phys. Rev. Lett.*, 105:018105, 2010.
- [47] K. Koshiyama and S. Wada. Molecular dynamics simulations of pore formation dynamics during the rupture process of a phospholipid bilayer caused by high-speed equibiaxial stretching. *Journal of Biomechanics*, 44(11):2053–2058, 2011.
- [48] S. Sun, J. T. Y. Wong, and T. Zhang. Molecular dynamics simulations of phase transition of lamellar lipid membrane in water under an electric field. *Soft Matter*, 7(1):147–152, 2011.
- [49] K. P. Santo and M. L. Berkowitz. Shock wave interaction with a phospholipid membrane: coarse-grained computer simulations. *The Journal of Chemical Physics*, 140(5):054906, 2014.
- [50] T. Shigematsu, K. Koshiyama, and S. Wada. Molecular dynamics simulations of pore formation in stretched phospholipid/cholesterol bilayers. *Chemistry and Physics of Lipids*, 183:43–49, 2014.
- [51] T. Shigematsu, K. Koshiyama, and S. Wada. Effects of stretching speed on mechanical rupture of phospholipid/cholesterol bilayers: molecular dynamics simulation. *Scientific Reports*, 5(15369), 2015.
- [52] M. A. Murphy, M. F. Horstemeyer, S. R. Gwaltney, T. Stone, M. LaPlaca, J. Liao, L. Williams, and R. Prabhu. Nanomechanics of phospholipid bilayer failure under strip biaxial stretching using molecular dynamics. *Modelling and Simulation in Materials Science and Engineering*, 24(5):055008, 2016.

- [53] S. A. Kirsch and R. A. Böckmann. Membrane pore formation in atomistic and coarse-grained simulations. *Biochimica et Biophysica Acta (BBA)-Biomembranes*, 1858(10):2266–2277, 2016.
- [54] L. Zhang, J. Jasa, G. Gazonas, A. Jérusalem, and M. Negahban. Extracting continuum-like deformation and stress from molecular dynamics simulations. *Computer Methods in Applied Mechanics and Engineering*, 283(0):1010–1031, 2015.
- [55] L. Zhang, Z. Zhang, J. Jasa, D. Li, R. O. Cleveland, M. Negahban, and A. Jérusalem. Molecular dynamics simulations of heterogeneous cell membranes in response to uniaxial membrane stretches at high loading rates. *Scientific Reports*, 7(8316), 2017.
- [56] Mark Tuckerman. *Statistical Mechanics: Theory and Molecular Simulation*. Oxford University Press, 2010.
- [57] Ellad B. Tadmor and Ronald E. Miller. *Modeling Materials: Continuum, Atomistic and Multiscale Techniques*. Cambridge University Press, 2011.
- [58] M. Karplus and J. A. McCammon. Molecular dynamics simulations of biomolecules. *Nature Structural Biology*, 9(9):646–652, 2002.
- [59] R. O. Dror, R. M. Dirks, J. P. Grossman, H. Xu, and D. E. Shaw. Biomolecular simulation: a computational microscope for molecular biology. *Annual Review of Biophysics*, 41(1):429–452, 2012.
- [60] T. Mori, N. Miyashita, W. Im, M. Feig, and Y. Sugita. Molecular dynamics simulations of biological membranes and membrane proteins using enhanced conformational sampling algorithms. *Biochimica et Biophysica Acta (BBA)-Biomembranes*, 1858(7, Part B):1635–1651, 2016.
- [61] J. B. Klauda, R. M. Venable, J. A. Freites, J. W. O’Connor, D. J. Tobias, C. Mondragon-Ramirez, I. Vorobyov, A. D. MacKerell, and R. W. Pastor. Update of the CHARMM all-atom additive force field for lipids: validation on six lipid types. *The Journal of Physical Chemistry B*, 114(23):7830–7843, 2010.

- [62] R.W Hockney and J.W Eastwood. *Computer Simulation Using Particles*. CRC Press, Taylor & Francis Group, 1988.
- [63] W. Humphrey, A. Dalke, and K. Schulten. VMD: visual molecular dynamics. *Journal of Molecular Graphics*, 14(1):33–38, 1996.
- [64] J. C. Phillips, R. Braun, W. Wang, J. Gumbart, E. Tajkhorshid, E. Villa, C. Chipot, R. D. Skeel, L. Kale, and K. Schulten. Scalable molecular dynamics with NAMD. *Journal of Computational Chemistry*, 26(16):1781–1802, 2005.
- [65] N. Kučerka, M. Nieh, and J. Katsaras. Fluid phase lipid areas and bilayer thicknesses of commonly used phosphatidylcholines as a function of temperature. *Biochimica et Biophysica Acta (BBA)-Biomembranes*, 1808(11):2761–2771, 2011.
- [66] N. Kučerka, S. Tristram-Nagle, and J. F. Nagle. Structure of fully hydrated fluid phase lipid bilayers with monounsaturated chains. *The Journal of Membrane Biology*, 208(3):193–202, 2006.
- [67] W. H. Grover, A. K. Bryan, M. Diez-Silva, S. Suresh, J. M. Higgins, and S. R. Manalis. Measuring single-cell density. *Proceedings of the National Academy of Sciences of the United States of America*, 108(27):10992–10996, 2011.
- [68] S. Plimpton. Fast parallel algorithms for short-range molecular dynamics. *Journal of Computational Physics*, 117(1):1–19, 1995.
- [69] D. Davydov and P. Steinmann. Reviewing the roots of continuum formulations in molecular systems. Part III: Stresses, couple stresses, heat fluxes. *Mathematics and Mechanics of Solids*, 20(10):1153–1170, 2013.
- [70] W. F. D. Bennett, N. Sapay, and D. P. Tieleman. Atomistic simulations of pore formation and closure in lipid bilayers. *Biophysical Journal*, 106(1):210 – 219, 2014.
- [71] M. Tarek. Membrane electroporation: A molecular dynamics simulation. *Biophysical Journal*, 88(6):4045 – 4053, 2005.



- [72] D. M. Zuckerman. Equilibrium sampling in biomolecular simulations. *Annual Review of Biophysics*, 40(1):41–62, 2011.
- [73] B. J. Berne and J. E. Straub. Novel methods of sampling phase space in the simulation of biological systems. *Current Opinion in Structural Biology*, 7(2):181–189, 1997.

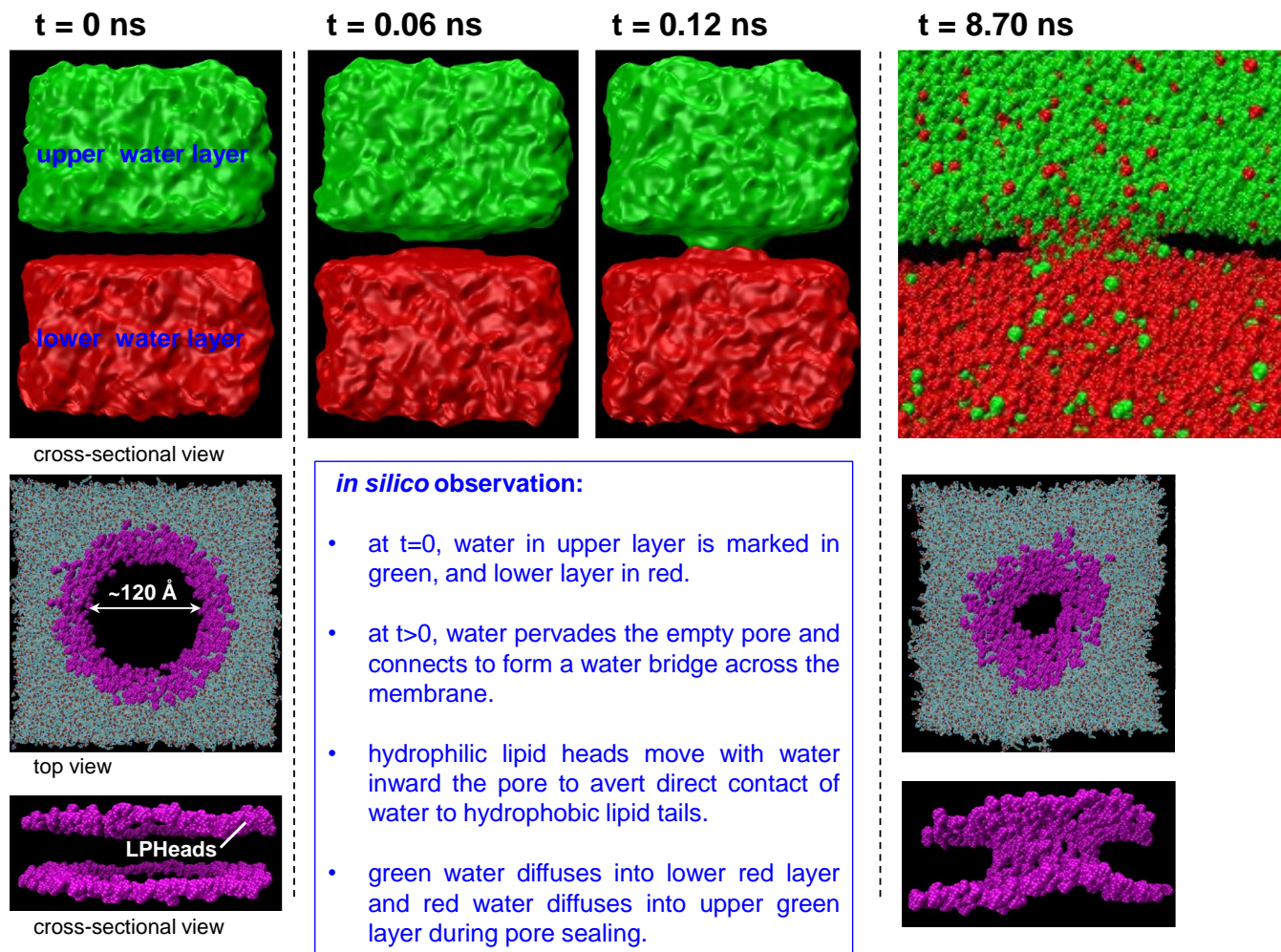


Figure 2: An ongoing membrane sealing process for a patch of hydrated POPC bilayer with a  $\sim 120$  Å-diameter pore captured by all-atom MD simulations. Top row: the motion of water is tracked by marking water molecules with different colours to distinguish which layer they originally belong to (green for upper layer and red for lower layer). The lipid molecules are visually hidden for clarity. Middle row: group LPHeads, represented as VDW in magenta, is assigned to the hydrophilic phosphate heads that are in the close vicinity of the pore. At time  $t = 8.70$  ns, the pore still remains open and sealing is in progress. Water is visually hidden for clarity. Bottom row: group LPHeads is visually highlighted to trace its movement. The pore wall has transformed from being hydrophobic at  $t = 0$  to hydrophilic at time  $t = 8.70$  ns.

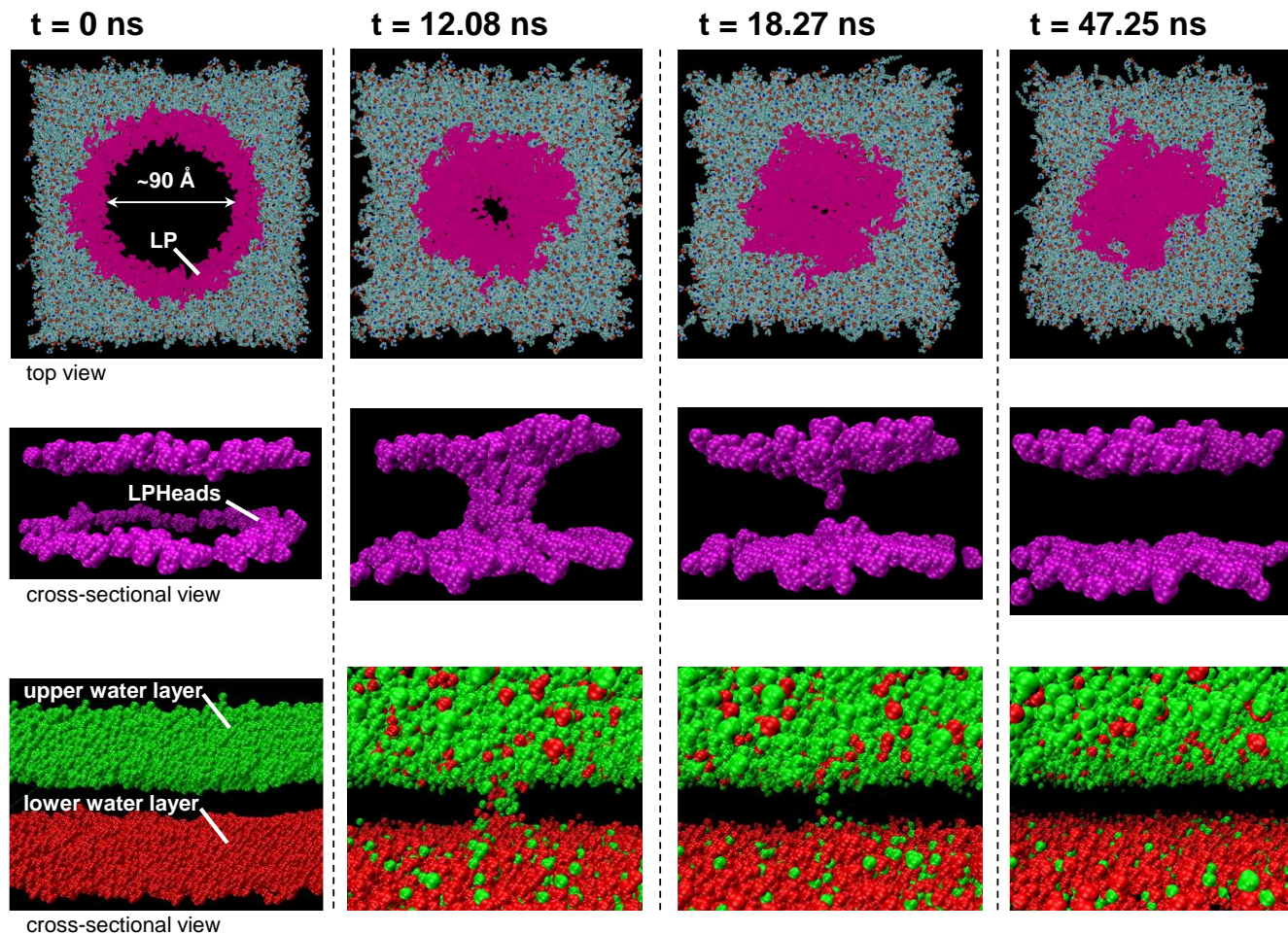


Figure 3: A complete membrane sealing process for a patch of hydrated POPC bilayer with a  $\sim 90$  Å-diameter pore captured by all-atom MD simulations. Top row: group LP, represented as Lines in colour magenta-process, is assigned to the lipid molecules surrounding the pore. The pore radius is reduced over time and has established a stable sealed conformation at the end of simulation ( $t = 47.25$  ns). Water is visually hidden for clarity. Middle row: group LPHeads is tracked to examine its structural alteration during sealing. At  $t = 12.08$  ns some of the lipid heads have bent over to form a hydrophilic pore wall. At  $t = 18.27$  ns most of the lipid heads have been forced out of the pore. At  $t = 47.25$  ns all of the lipid heads have rearranged into two planar sealed leaflets. Bottom row: at  $t = 12.08$  ns a water bridge across the membrane has been built with molecules from both layers. Transfer of water through the pore from one layer to the other is then in progress. At  $t = 18.27$  ns the water bridge is almost annihilated as the pore radius decreases. At  $t = 47.25$  ns all of the water molecules have been completely pushed out of the pore as the membrane has fully sealed.

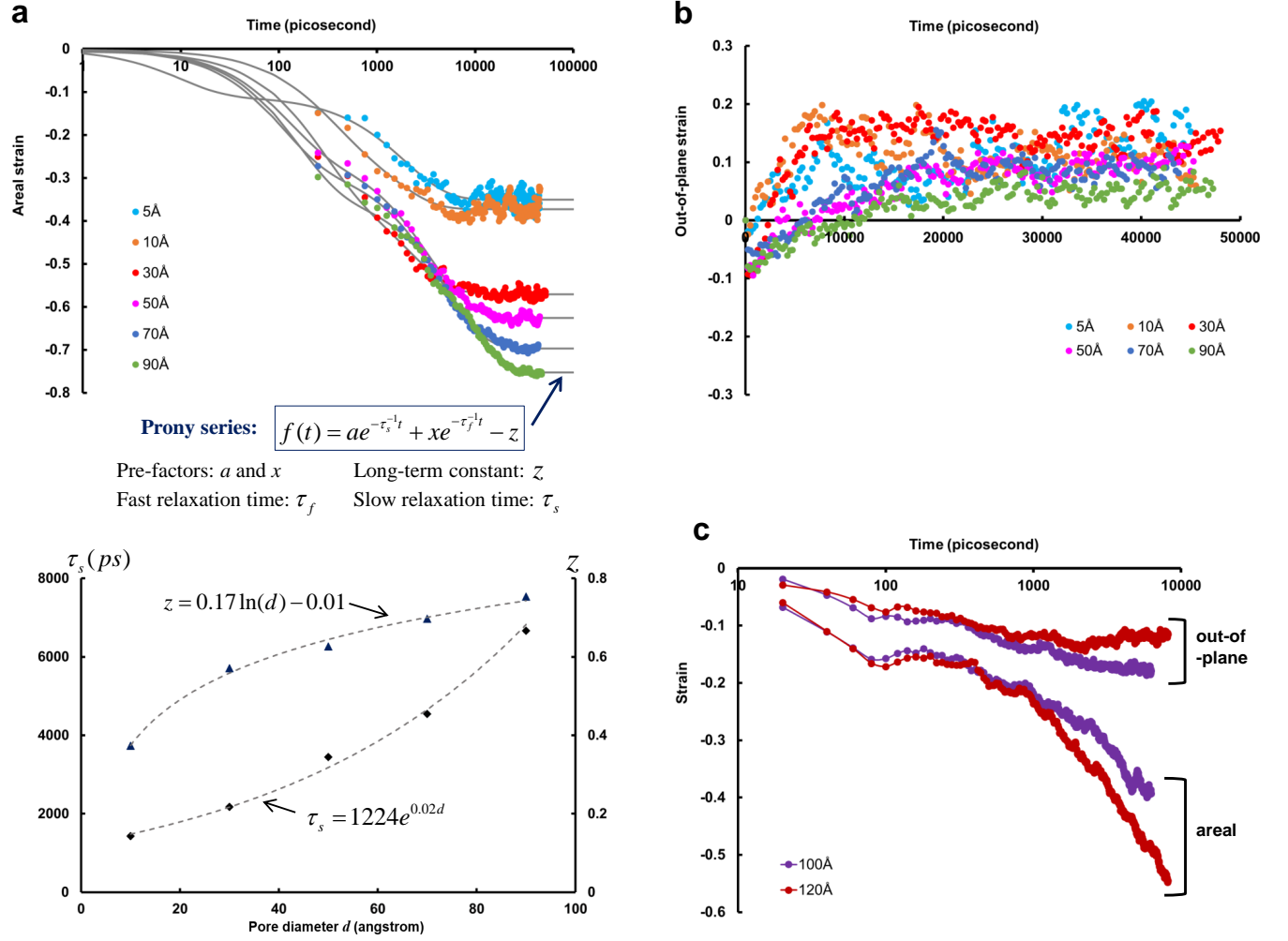


Figure 4: Membrane's continuum-like deformation characteristics over the course of pore sealing. Time evolution of (a) in-plane areal strain and (b) out-of-plane strain experienced by the lipid molecules (group LP) encompassing the pore (with diameter  $\leq 90$  Å). (a) also includes the curve fitting with Prony series whose slow relaxation time  $\tau_s$  and long-term constant  $z$  exhibit pore-size dependence. (c) In-plane areal and out-of-plane strain histories (up to 8.70 ns) of the hydrophilic phosphate heads (group LPHeads) adjacent to the pore (with diameter  $\geq 100$  Å).



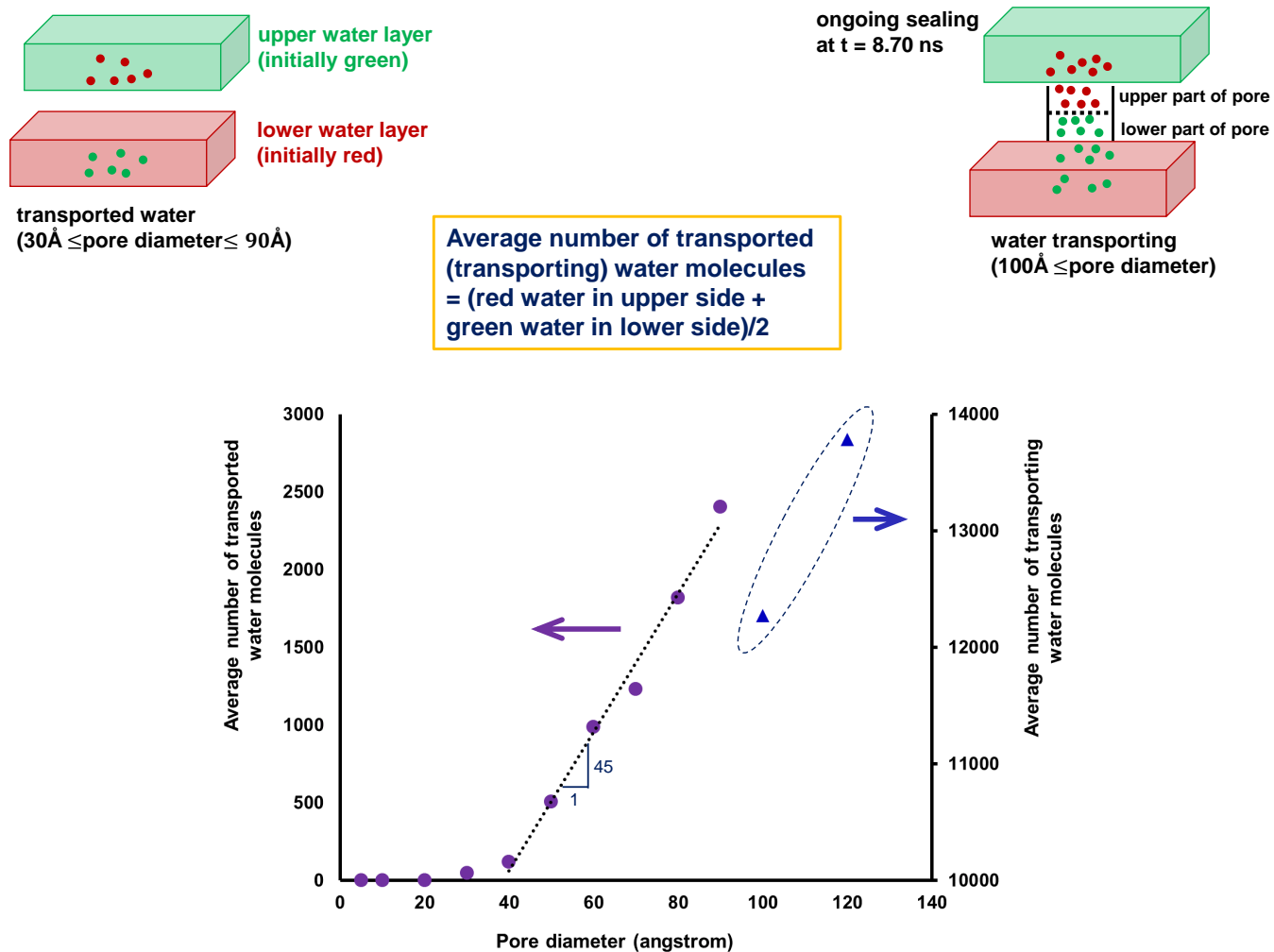


Figure 5: Quantification of water permeation through pores of various sizes to the opposite sides. No water transport is observed for pores with diameters  $\leq 20\text{ \AA}$ . For pores with diameters  $\leq 90\text{ \AA}$ , the number of water molecules that have diffused from their initial layers to the opposite layers in the fully sealed configuration is estimated by tracking their IDs and then averaged between the two sides. For pores with diameters  $\geq 100\text{ \AA}$ , the number of water molecules that are penetrating from their initial layers to the opposite sides (including the opposite parts of the pore) at time  $t = 8.70\text{ ns}$  is approximated by tracking their IDs and then averaged between the two sides.

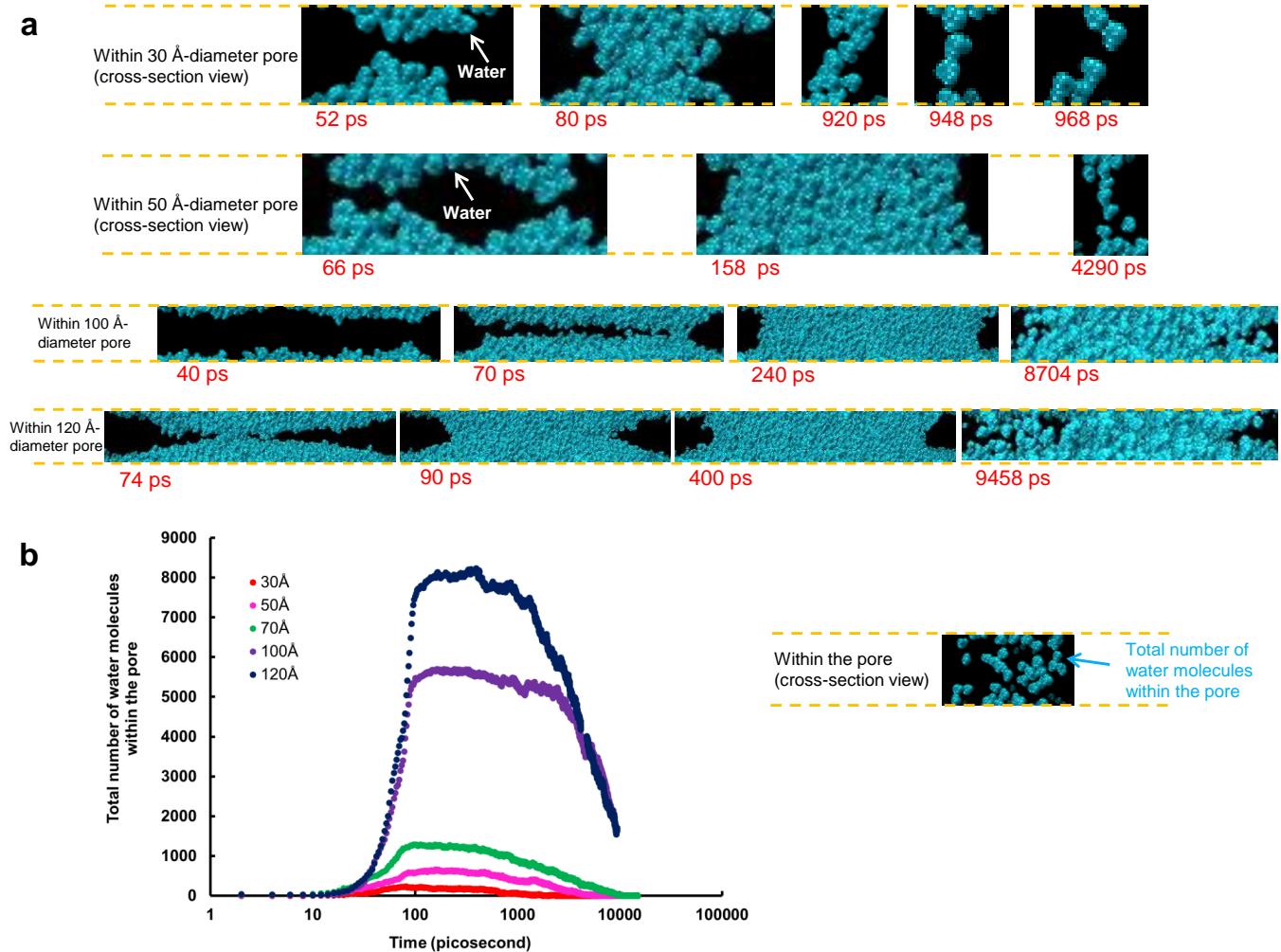


Figure 6: (a) Representative simulation close-ups of the configurations of water molecules within the pore domains over the course of membrane sealing. Only the water molecules within the pore are represented as VDW in cyan, with the remainder of the system visually hidden. (b) Time evolution of the total number of water molecules within the pore of various initial sizes ( $\sim 30$  Å- $120$  Å in diameter).